

Decay of mass-separated $^{183}\text{Pt}^m$ (43 s) and $^{183}\text{Pt}^g$ (6.5 min) to ^{183}Ir

K. Jentoft-Nilsen* and J. L. Wood

School of Physics, Georgia Institute of Technology, Atlanta, Georgia 30332-0430

J. von Schwarzenberg

Department of Physics, University of Notre Dame, Notre Dame, Indiana 46556

(Received 30 April 1998)

The decays of $^{183}\text{Pt}^m$ (43 s, $J^\pi = \frac{7}{2}^-$) and $^{183}\text{Pt}^g$ (6.5 min, $J^\pi = \frac{1}{2}^-$) have been studied with mass-separated sources from the UNISOR facility. Multiscaled spectra of γ rays, x rays, and conversion electrons, as well as $\gamma\gamma t$, $\gamma X t$, $e\gamma t$, and $eX t$ coincidences, were obtained. A revision of the low-lying positive-parity states is necessary in order to accommodate a strong 58 keV transition which is previously unreported. Other additions are made to the low-energy part of the ^{183}Ir scheme. The systematic features of the neutron-deficient odd-mass Ir isotopes are discussed. [S0556-2813(99)06005-7]

PACS number(s): 21.10-k, 27.70.+q, 23.20.Lv, 23.20.Nx

I. INTRODUCTION

The neutron-deficient odd-mass Ir isotopes lie along the heavy-mass border of the deformed ‘‘rare-earth’’ region. The low-lying states are well described in terms of Nilsson states and axially symmetric rotations. In particular, detailed studies of ^{185}Ir by radioactive decay of $^{185}\text{Pt}^{m,g}$ [1] and in-beam reaction γ -ray spectroscopy [2] and of ^{181}Ir by radioactive decay of ^{181}Pt [3] and in-beam spectroscopy [4] have been made. However, information on excited states in ^{183}Ir is far more limited and is confined to a few details of the radioactive decay of $^{183}\text{Pt}^m$ [5], an unpublished study of $^{183}\text{Pt}^g$ decay [6], and two in-beam studies [7,8] that identify a few bands but are not in complete agreement.

The present investigation was undertaken as part of a detailed spectroscopy study [9,10] of the $A = 183$ decay chain. In particular, the use of conversion-electron spectroscopy in coincidence with γ rays provides a powerful method for identifying low-energy transitions and for determining conversion-electron subshell intensity ratios which lead to reliable transition multipolarities. The present work illustrates this method.

II. EXPERIMENTAL PROCEDURE

Sources of $^{183}\text{Pt}^{m,g}$ were obtained from the radioactive decay of ^{183}Au (42 s) following the $^{181}\text{Ta}(^{12}\text{C}, 10n)$ reaction and mass separation on line with the University Isotope Separator at Oak Ridge (UNISOR). The ^{181}Ta target, consisting of a stack of thin self-supporting foils with a total thickness of 47 mg/cm^2 , was mounted inside the UNISOR version of the FEBIAD-F ion source [11] and bombarded with 165 MeV $^{12}\text{C}^{6+}$ ions from the Holifield Heavy Ion Research Facility (HHIRF) 25 MV tandem accelerator. Sources were collected on aluminized Mylar tape for a preset time and moved by a tape transport system [12] to two sequential counting stations. The experimental arrangement

was such that a source was being counted at each counting station while a third source was being collected. Source collection times were 32 s each.

The use of two counting stations allowed the simultaneous acquisition of γ -ray and conversion-electron time-sequenced spectra, and $\gamma\gamma t$, $\gamma X t$, $e\gamma t$, and $eX t$ coincidence data. The first counting station, consisting of an ORTEC Gamma-X detector with 25% efficiency (resolution 1.9 keV at 1063 keV) placed at 180° to a customized KeveX Si(Li) electron spectrometer ($3 \text{ mm} \times 200 \text{ mm}^2$ surface area, resolution 2.1 keV at 975 keV), acquired and stored both singles and coincidence data event by event on magnetic tape. The second counting station, consisting of a 15% ORTEC Gamma-X detector (resolution 2.0 keV at 1332 keV), placed at 180° to a 17% Ge(Li) detector (resolution 2.6 keV at 1332 keV) collected and stored both singles and $\gamma\gamma$ and γX coincidence data event by event on magnetic tape. The tapes were scanned subsequently for selected energy and time gates.

The photon detectors were calibrated for energy and intensity with a standardized NBS/NIST calibrated mixed γ -ray source (containing ^{125}Sb , ^{154}Eu , and ^{155}Eu). The electron spectrometer was energy calibrated with a ^{207}Bi source, while the efficiency was determined from measurement of the conversion coefficient for a known $E2$ transition in the decay of ^{183}Pt to ^{183}Ir acquired during the experiment. All calibration standards were placed in the same counting geometry as the sources collected during the experiment. Typical source-to-detector distances were 1–2 cm. The time-to-amplitude converter (TAC) spectra for the $\gamma\gamma$ and γe coincidence measurements exhibited full widths at half maximum (FWHM) of $\approx 15 \text{ ns}$ and $\approx 30 \text{ ns}$, respectively.

The γ -ray spectra were taken in the energy range 40–3200 keV. Conversion-electron spectra were taken in the range 25–1610 keV. In scanning the event-by-event coincidence data on tape, time gates were set with $\approx 70 \text{ ns}$ widths for both $\gamma\gamma t$ and $e\gamma t$ coincidence events. This gave true-to-chance ratios of $\approx 50:1$.

III. EXPERIMENTAL RESULTS

The results presented here were extracted from data sets that contained both ^{183}Au and $^{183}\text{Pt}^{m,g}$ decay information.

*Present address: American Institute of Physics, One Physics Ellipse, College Park, Maryland 20740-3843.

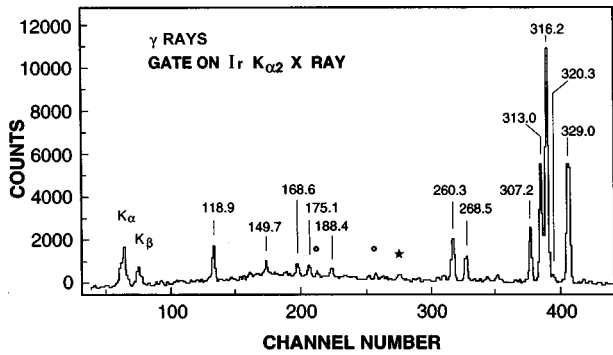


FIG. 1. Gamma-ray spectrum in coincidence with Ir $K\alpha_2$ x rays showing lines between 45 and 355 keV. The circles over lines at 179 and 214 keV indicate two of the strongest lines in the $^{183}\text{Au} \rightarrow ^{183}\text{Pt}$ decay. The star over the line at 229 keV is one of the strongest lines in the $^{183}\text{Ir} \rightarrow ^{183}\text{Os}$ decay. The lines at 313, 316, and 329 keV are strong lines in the $^{183}\text{Pt}^m$ (43 s) decay. The lines at 119, 260, 269, and 307 keV are strong lines in the $^{183}\text{Pt}^g$ (6.5 min) decay.

Thus, all illustrative spectra are coincidence gated. Figure 1 shows an Ir $K\alpha_2$ x-ray gated γ -ray spectrum covering the energy range 45–355 keV. Contamination from ^{183}Au decay and a trace of ^{183}Ir (55 min) decay is just discernible. Gamma rays from the decay of ^{183}Au were identified using a separate analysis [9] of these data sets and the study of Rousière *et al.* [13] (between which there is good agreement). Gamma rays from the decay of ^{183}Ir were identified using data from [14]. No contamination from neighboring mass chains or room background was seen in coincidence.

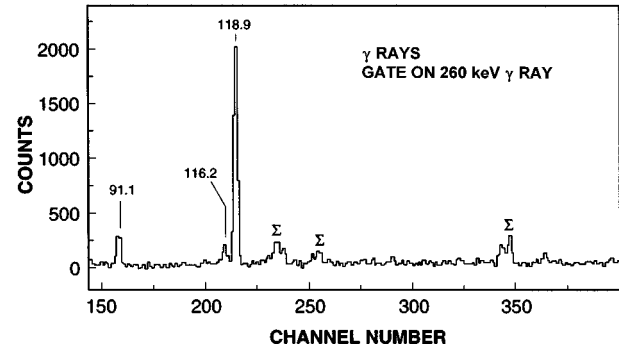
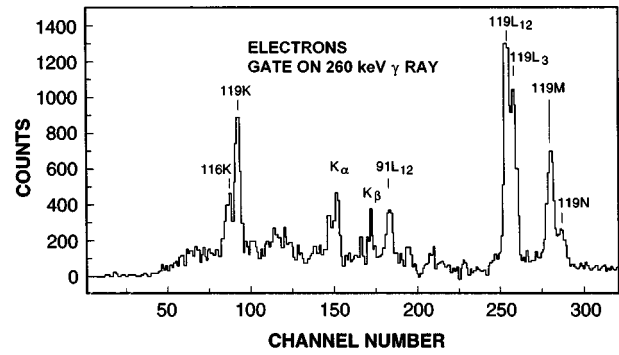


FIG. 3. Gamma rays and corresponding conversion electrons in coincidence with the 260 keV γ -ray transition. The electron subshell lines corresponding to the 119 keV transition establish the 119 keV transition as pure $E2$ (see the text for a further discussion of the 119 keV transition). The γ -ray lines marked by Σ are sum peaks.

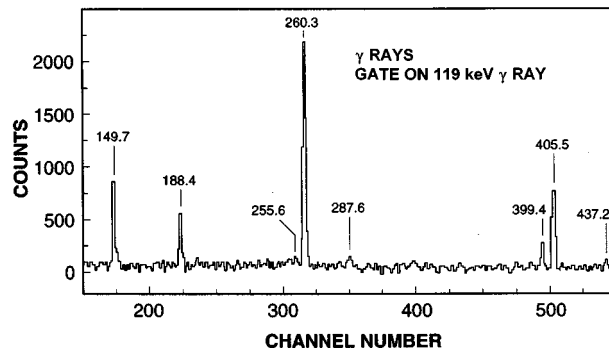
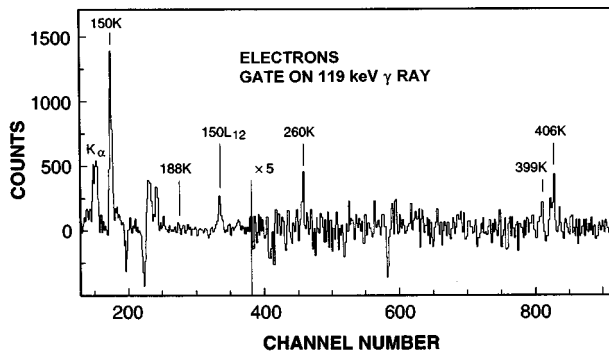


FIG. 2. Gamma rays and corresponding conversion electrons in coincidence with the 119 keV γ -ray transition. The 188 and 260 keV transitions have $E1$ multipolarity (cf. Table II). The spectral features between the 150 K and 188 K electron lines are Compton backscatter artifacts due to $^{183}\text{Au} \rightarrow ^{183}\text{Pt}$ decays in the source.

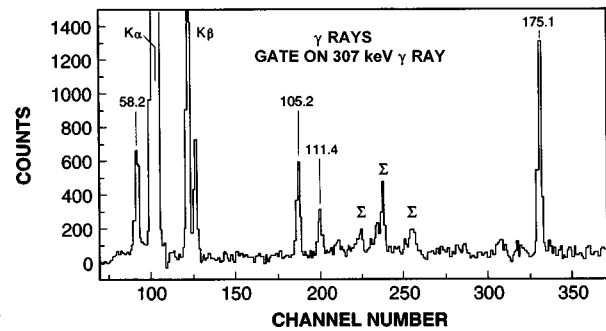
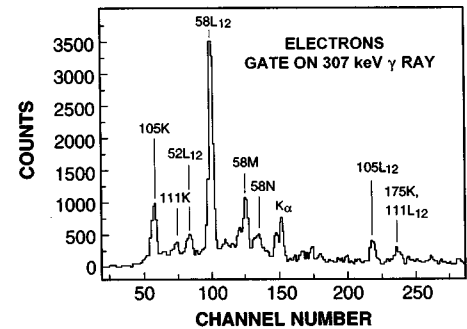


FIG. 4. Gamma rays and corresponding conversion electrons in coincidence with the 307 keV γ -ray transition. The 58 keV transition, which feeds the 307 keV level is observed for the first time in this work and is discussed in the text. The 175 keV transition has $E1$ multipolarity and thus is only weakly converted.

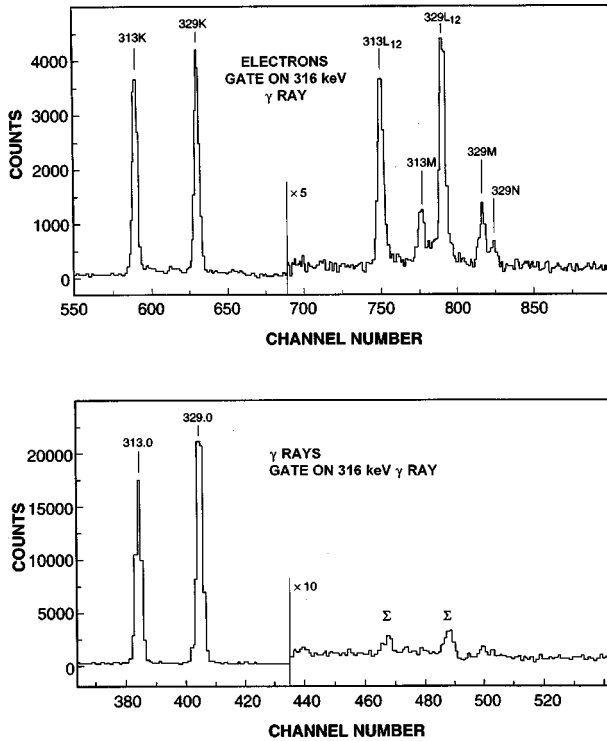


FIG. 5. Gamma rays and corresponding conversion electrons in coincidence with the 316 keV γ -ray transition.

Our data are dominated by the $^{183}\text{Pt}^m$ (43 s) decay which results in the strong γ -ray lines seen in Fig. 1 above 300 keV. The $^{183}\text{Pt}^g$ (6.5 min) decay is much weaker in our data because of the short collection time (32 s) of the sources (which was optimized for the study of the ^{183}Au isobar). The strongest line from $^{183}\text{Pt}^g$ that appears in Fig. 1 is at 118.9 keV. Gamma-ray lines from the decay of $^{183}\text{Pt}^g$ were identified with the help of the unpublished study of Zerrouki [6]. However, we see all of the lines belonging to the $^{183}\text{Pt}^g \rightarrow ^{183}\text{Ir}$ decay that were reported by Zerrouki even though we did not optimize the present study for $^{183}\text{Pt}^g$.

Selected spectra from the $\gamma\gamma t$ and $e\gamma t$ coincidences are shown in Figs. 2–9. It was possible to identify x-ray lines uniquely in nearly all coincidence gates, providing a confirmation of our assignment of γ rays to $^{183}\text{Pt}^{m,g}$ decays. Spurious events due to Compton backscattering (cf. Fig. 2) and summing (cf. Figs. 3–5 and 7) were identified and eliminated. Coincidence intensities were extracted for all lines seen in the coincidence gates.

The energies, intensities, coincidence assignments, and decay scheme location of γ rays assigned to the $^{183}\text{Pt}^{m,g}$ decays are listed in Table I. Intensities of conversion-electron lines and transition multipolarities for the $^{183}\text{Pt}^{m,g}$ decays are listed in Table II. The γ -ray intensities are deconvoluted into $^{183}\text{Pt}^m$ (high-spin) and $^{183}\text{Pt}^g$ (low-spin) components using the data of Zerrouki which are given in Table I. We note that in Zerrouki's data set, lines belonging to $^{183}\text{Pt}^g(\alpha)^{179}\text{Os}(\beta)^{179}\text{Re}$ are erroneously included. These lines are not included in Table I. The deconvolution process was rapidly convergent because the ratio $^{183}\text{Pt}^m:^{183}\text{Pt}^g$ in our data set differs by a factor of 24 from that of Zerrouki (cf. Table I, I_γ^c and I_γ^d for the 316.2, 629.6, and 645.2 keV γ

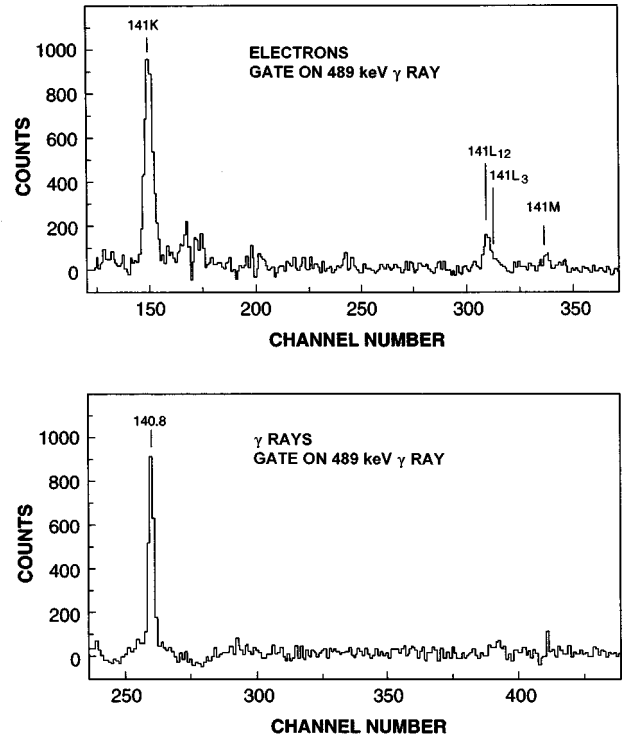


FIG. 6. Gamma rays and corresponding conversion electrons in coincidence with the 489 keV γ -ray transition. This establishes a new member of the ground-state band with $J^\pi = \frac{1}{2}^-$ (cf. Fig. 10).

rays). Some aspects of the deconvolution process are discussed further in Sec. IV.

The electron intensities in Table II are normalized to the γ -ray intensities through the 119 keV transition α_K value. This is fixed at the theoretical value for a pure $E2$ transition because the L_{12}/K , L_3/K , and M/K subshell ratios for the 119 keV transition (cf. Fig. 3) unequivocally support this assignment. Conversion coefficients and multipolarities for some transitions are reported also by Zerrouki. The agreement with our results is good. In particular, we concur on the assignment of $E1$ multipolarity to the 188.4, 260.3, and 307.2 keV transitions. We also tentatively assign $E1$ multipolarity to the newly observed transition of 175.1 keV. This transition is discussed further in the next section.

IV. DECAY SCHEMES

Our decay scheme for 43 s $^{183}\text{Pt}^m \rightarrow ^{183}\text{Ir}$ is shown in Fig. 10 and for 6.5 min $^{183}\text{Pt}^g \rightarrow ^{183}\text{Ir}$ is shown in Fig. 11. These schemes rely almost totally on the coincidence data. Figure 5, which contains the strongest coincidences observed in this work, indicates the overall statistical quality of our data. The coincidences which are important to the elucidation of the schemes are shown in Figs. 2, 4, and 6–9. The schemes possess low-lying positive- and negative-parity states. Four $E1$ transitions, the 175.1, 188.4, 260.3, and 307.2 keV transitions, are observed to interconnect them. The comparison of the electron to γ -ray intensities in Fig. 2 clearly reveals the $E1$ character of the 188.4 and 260.3 keV transitions. Further, the 188.4 and 307.2 keV $E1$ transitions fix the spin of the lowest-lying positive-parity state as $J = \frac{3}{2}$. A number of new low-lying states are established in this work. The

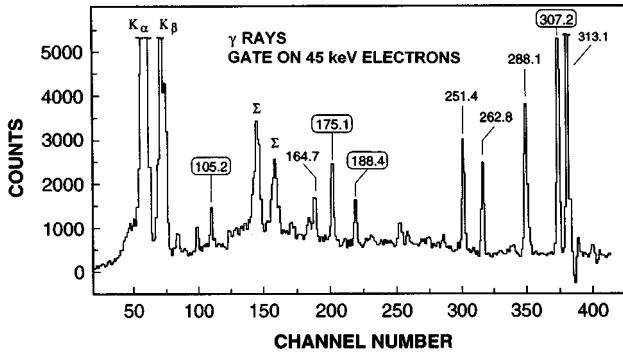


FIG. 7. Gamma rays in coincidence with the 45 keV electrons. The gating electrons correspond to L electrons from the (new) 58 keV transition together with 124 K and 48 M electrons from the $^{183}\text{Au} \rightarrow ^{183}\text{Pt}$ decay. The γ rays in coincidence with the 58 keV transition are shown in boxes. The 105 keV transition is discussed further in the text.

lowest-lying new negative-parity state is the $J^\pi = \frac{1}{2}^-$ state at 504.7 keV. This state is fed by the very strongly populated $J^\pi = \frac{9}{2}^-$ state at 645.4 keV. The evidence for this is shown in Fig. 6. The lowest-lying new positive-parity state is at 365.4 keV and deexcites by a strong 58 keV transition which has not been observed previously. The location of this transition is discussed in more detail below.

The $^{183}\text{Pt}^g \rightarrow ^{183}\text{Ir}$ scheme is substantially in agreement with Zerrouki. A number of points should be noted regarding the present work and that of Zerrouki. Although the present work compared to that of Zerrouki was far from optimum for the study of the decay scheme of low-spin ^{183}Pt , all the lines reported by Zerrouki were seen in the present work. Further, the relative intensities of γ -ray transitions directly deexciting a common level are, for the most part, in good agreement between the two studies; cf. I_γ^c and I_γ^d in Table I. Disagreement occurs where Zerrouki indicated contaminant lines: these are so indicated in Table I, i.e., the lines at 227, 252.1, 255.6, and 556.2 keV. In all instances we can establish relative intensities for these transitions from other γ rays deexciting common levels. There are four lines for which we used γ -ray spectra presented by Zerrouki to ascertain their intensities in the low-spin decay: these are so indicated in Table I, i.e., the lines at 58.2, 91.1, 105.2, and 470.3 keV. We assign

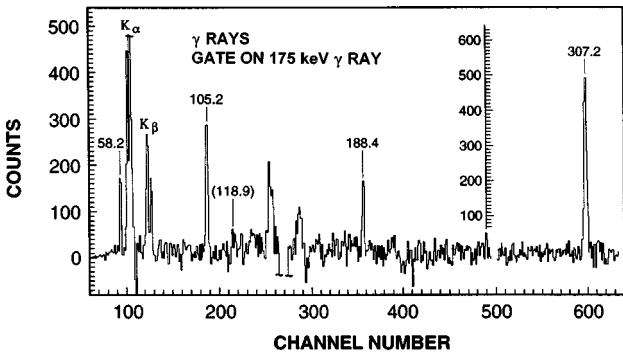


FIG. 8. Gamma rays in coincidence with the 175 keV γ -ray transition. This illustrates the decay path from the 645.4 keV ($J^\pi = \frac{9}{2}^-$) level via the 175 keV $E1$ transition to the 470.5 keV ($J^\pi = \frac{7}{2}^+$) level which is deexcited by the (reassigned) 105 keV transition seen in beam.

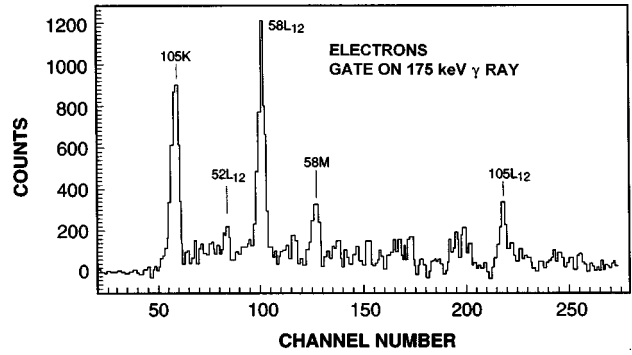


FIG. 9. Conversion electrons in coincidence with the 175 keV γ -ray transition. (cf. Fig. 8).

large errors to the deduced low-spin intensities for these lines. (The subscheme in Zerrouki's work which is identifiable as belonging to the $^{179}\text{Os} \rightarrow ^{179}\text{Re}$ decay, so noted above, is not connected by him to the bona fide $^{183}\text{Pt}^g \rightarrow ^{183}\text{Ir}$ scheme.) The $^{183}\text{Pt}^m \rightarrow ^{183}\text{Ir}$ scheme confirms and considerably extends the work of Visvanathan *et al.* [5]. The levels in ^{183}Ir populated in the decay of $^{183}\text{Pt}^m$ (high spin) exhibit some commonality with in-beam γ -ray studies of Janzen *et al.* [7] and Kreiner *et al.* [8]. However, on one crucial point our scheme differs from both of these in beam studies. This is detailed below.

We observe, for the first time, a 58 keV transition in ^{183}Ir . This transition is located between the (positive-parity) states at 307.2 and 365.4 keV and is shown in both Figs. 10 and 11. The evidence for this assignment is supported by the 307 $\gamma\gamma$ and 307 γe data; cf. Fig. 4. Further, we locate a 105.2 keV transition as feeding the 365.4 keV level. The evidence for this is presented in Figs. 7, 8, and 9. The strength of the 58 keV transition (cf. Fig. 4) requires that it directly feed the 307.2 keV level. The key to correctly locating the 105.2 keV transition (as feeding the 365.4 keV level) comes from the 175.1 keV transition (cf. Figs. 8 and 9) which we assign as deexciting the very strongly populated $J^\pi = \frac{9}{2}^-$ state at 645.4 keV. The ordering of the 105.2 and 175.1 keV transitions in coincidence with the 175.1 keV transition (cf. Fig. 9). The 105.2 keV transition seen in this work is very probably the 105 keV transition seen in the in-beam studies [7,8] and assigned as directly feeding the 307.2 keV level. Consequently, we propose that the entire band reported in [7,8] including the 105 keV transition be displaced upwards by 58 keV. This is discussed further in the next section.

We adopt the Nuclear Data Sheets assignments [15] for the ground state spin parities of ^{183}Ir , $^{183}\text{Pt}^g$, and $^{183}\text{Pt}^m$, i.e., $J^\pi = \frac{5}{2}^-$, $\frac{1}{2}^-$, and $\frac{7}{2}^-$, respectively. The J^π assignments to $^{183}\text{Pt}^m$ and $^{183}\text{Pt}^g$ are supported by the observation [16] of an $M3$ isomeric transition in ^{183}Pt . (We note that this $M3$ transition, which cannot be coincidence gated, is too weak to have been seen in our data.) The determination of spin parities for excited states in ^{183}Ir is based on assigned multiplicities of transitions populating and depopulating each level, constrained by the spin parities of $^{183}\text{Ir}^g$ and $^{183}\text{Pt}^{m,g}$ (as noted above), by the relative population in the high-spin and low-spin ^{183}Pt beta decay, and by the population of states in ^{183}Ir observed using in-beam reaction γ -ray spectroscopy [7,8]. Further, we adopt the assignment $J^\pi = \frac{9}{2}^-$ for the 645.4

TABLE I. Gamma-ray data for the decay of $^{183}\text{Pt}^{m,g}$.

$E_\gamma(\Delta E_\gamma)^a$	E_i^b	E_f^b	$I_\gamma(\Delta I_\gamma)^c$	$I_\gamma(\Delta I_\gamma)^d$	$I_\gamma(\Delta I_\gamma)^g$	$I_\gamma(\Delta I_\gamma)^k$
52.0	x 470.5	418.4 x				i
58.2	x 365.4	307.2 x	12 (4)	$\leq 0.7^e$	≤ 0.7	0.7 (2)
91.1	x 470.3	379.2 x	3 (1)	2.8 (14) ^e	1.4 (5)	0.11 (6)
105.2	x 470.5	365.4 x	9 (2)	0.9 (6) ^e	0.5 (3)	0.49 (12)
111.4	x 418.4	307.2 x	5 (1)	1 (0.5)	1.2 (5)	0.23 (6)
116.2	586.5	470.3 x	12(3)			0.09 (4)
118.9	x 118.9	0.0	100 (7)	100	100	[1.2 (8)] ^j
140.8	645.4	504.7 x	17 (3)			1.0 (2)
143.7	667.9	524.4 x	2 (1)		1.3 (6)	0.02 (2)
149.7	x 268.5	118.9 x	38 (3)	33 (3)	32 (3)	0.3 (2)
163	470.3	307.2 x	2 (1)		2 (1)	0.15 (8)
168.6	x 184.6	16.0	19 (4)	< 4		1.1 (2)
175.1	645.4	470.5 x	28 (4)			1.6 (2)
188.4	x 307.2	118.9 x	30 (4)	18 (3)	16 (3)	0.9 (2)
196.6	842.0	645.4 x	13 (4)			0.7 (2)
227	556.2	329.0 x	6 (1)	[15 (4)] ^f	2 (1)	0.23 (6)
252.1	776.3	524.4 x	3 (1)	[5 (2)] ^f	4 (1)	
255.6	524.4	268.5 x	16 (3)	[8 (2)] ^f	9 (2)	0.3 (1)
260.3	x 379.2	118.9 x	104 (6)	90 (15)	90 (15)	0.8 (8)
268.5	x 268.5	0.0	80 (12)	80 (10)	80 (10)	0.6 (4)
279.3	586.5	307.2 x	3 (1)			0.2 (1)
281.5	(1309.1	1027.6) x	10 (5)			0.6 (3)
287.6	556.2	268.5 x	17 (3)	9 (2)	6 (1)	0.6 (2)
289.8	597.0	307.2 x	8 (2)			0.5 (1)
307.2	x 307.2	0.0	197 (10)	97 (10)	93 (10)	6.0 (9)
313.0	x 329.0	16.0	456 (70)	[31] ^f	8	26 (4)
316.2	x 645.4	329.0 x	1018 (55)	43		59 (3)
320.3	x 504.7	184.6 x	15 (4)			0.9 (2)
329.0	x 329.0	0.0	593 (90)	34	10	34 (5)
382.2	x(1027.6	645.4) x	13 (7)			0.8 (4)
399.4	x 667.9	268.5 x	36 (2)	31 (7)	27 (7)	0.3 (3)
405.5	x 524.4	118.9 x	42 (5)	29 (6)	28 (6)	0.8 (4)
418.3	x 418.4	0.0	25 (5)	9 (2)	8 (2)	1.0 (3)
424.1	753.1	329.0 x	8 (3)			0.5 (2)
437.2	556.2	118.9 x	6 (2)		2 (1)	0.2 (1)
461.2	x 645.4	184.6	13 (6)			0.8 (4)
470.3	x 470.3	0.0	19 (7)	9 (8) ^e	8 (3)	0.7 (3)
488.6	x 504.7	16.0	58 (5)			3.4 (3)
524.5	524.4	0.0	13 (6)	9 (2)	8 (2)	0.2 (1)
549.0	667.9	118.9 x	27 (8)	23 (5)	20 (5)	0.2 (2)
556.2	556.2	0.0	32 (10)	[11 (2)] ^f	11 (2)	1.3 (6)
564.5	(893.5	329.0) x	5 (2)			0.2 (1)
570.6	(877.8	307.2) x	10 (5)			0.4 (2)
578.9	997.3	418.4 x	5 (2)		3 (2)	0.2 (1)
618.8	997.3	379.2 x	8 (3)	10 (3)	8 (3)	0.2 (1)

TABLE I. (Continued).

$E_\gamma(\Delta E_\gamma)^a$	E_i^b	E_f^b	$I_\gamma(\Delta I_\gamma)^c$	$I_\gamma(\Delta I_\gamma)^d$	$I_\gamma(\Delta I_\gamma)^e$	$I_\gamma(\Delta I_\gamma)^k$
629.6	x645.4	16.0	1800 (80)	74		100
633	997.3	365.4	5 (3)		3 (2)	0.2 (1)
642.4	1112.7	470.3 x	22 (4)	4 (2)	3 (2)	1.1 (2)
645.4	x645.4	0.0	371 (20)	15		21.5 (12)
657.4	776.3	118.9 x	24 (2)	26 (5)	26 (5)	
667.9	x667.9	0.0	40 (13)	27 (6)	26 (6)	0.3 (3)
690.1	997.3	307.2 x	10 (2)	5 (2)	5 (2)	0.3 (1)
708.8	1088.0	379.2 x	6 (2)	5 (1)	5 (1)	0.05 (5)
728.7	997.3	268.5 x	13 (4)	4 (2)	6 (3)	0.4 (2)
777.7	(1156.9	379.2)x	12 (3)	obs.	12 (3)	
790.8			19 (5)			1.1 (3)
868.2	1248.0	379.2 x	2 (1)	2	2 (1)	
923.3	1302.5	379.2 x	5 (2)	obs.	5 (2)	
941.3	1248.0	307.2 x	6 (2)	obs.	6 (2)	
1024.6	1331.8	307.2 x	5 (3)	6 (2)	6 (2)	
1115.5	(1585.8	470.3)x	16 (4)			0.9 (2)
1128.6	1774.0	645.4 x	30 (5)			1.7 (3)
1377.2	(1756.4	379.2)x	18 (6)	9 (3) ^h	8 (3)	0.6 (3)
1612.6	(2258.0	645.4)x	19 (7)			1.1 (4)
1730.0	2397.9	667.9 x	23 (6)			
1753.3	2258.0	504.7 x	8 (3)			0.4 (2)
1868.2	(2338.5	470.3)x	20 (6)			
2031.4	2338.5	307.2 x	5 (2)			
2112	2491	379.2 x	6 (2)			
2215	2594	379.2 x	5 (2)			
2221.7	2490.2	268.5 x	23 (5)			
2222.7	2529.9	307.2 x	5 (2)			

^a ΔE_γ values are ± 0.2 keV for $I_\gamma > 20$ and ± 0.4 keV for $I_\gamma < 20$ (column 4).
^bAn ‘‘x’’ to the left indicates a feeding coincidence; an ‘‘x’’ to the right indicates a deexciting coincidence. Assignments in parentheses are tentative.
^cIntensity of undeconvoluted γ -ray line determined in the present study.
^dIntensity taken from Zerrouki [6].
^eIntensity estimated from singles spectrum shown in [6].
^fLine indicated by Zerrouki [6] to be contaminated.
^gGamma-ray intensity for $^{183}\text{Pt}^g$ ($T_{1/2} = 6.5$ min, $J^\pi = \frac{1}{2}^-$) decay.
^hThe γ -ray spectrum in [6] has a high-energy cutoff of 1480 keV.
ⁱOnly seen in conversion electron spectrum.
^jIntensity estimated from feeding.
^kGamma-ray intensity for $^{183}\text{Pt}^m$ ($T_{1/2} = 43$ s, $J^\pi = \frac{7}{2}^-$) decay.

keV level, based on the fast beta decay to this level from $^{183}\text{Pt}^m$, as proposed by Visvanathan *et al.* [5]. We especially note the decay of the 645.4 keV level to the 504.7 keV level (cf. Fig. 6) and the 470.5 keV level (cf. Figs. 8 and 9). The 175.1 keV transition, connecting the 645.4 ($\frac{9}{2}^-$) and 470.5 ($\frac{7}{2}^+$) levels, has a K -conversion coefficient consistent with E1 multipolarity.

Our scheme is consistent with the systematics of the neighboring odd-mass Ir isotopes (cf. the next section). We estimate our scheme to be complete up to at least 600 keV

excitation energy. The only feature which appears to have poor consistency with the spin-parity assignments is the low-spin ^{183}Pt β feeding of the $\frac{7}{2}^-$ level at 329.0 keV. The intensity seems high considering that we do not see much secondary feeding of the level. However, we note that our feeding intensities depend on deconvolution of the high- and low-spin ^{183}Pt decays using Zerrouki’s data compared to ours. For the 329.0 keV level this involves the 313.0 and 329.0 keV transitions for which Zerrouki does not quote intensity errors (cf. Table I). Further, Zerrouki notes that in his work the 313.0 keV transition is unresolved from a strong

TABLE II. Internal conversion electron data for the decay of $^{183}\text{Pt}^{m,g}$.

E_γ (keV)	$I_\gamma(\Delta I_\gamma)$	$I_e(\Delta I_e)$	Experiment		Theory ^a		Multipolarity
					$M1$	$E2$	
52.0		6 (3)		L_{12}	5.83	33.9	$E2 (+ M1)$
			0.58 (20)	M/L_{12}	0.232	0.517	
58.2	12 (4)	60 (20)	5.0 (24)	$\alpha_{L_{12}}$	4.18	19.7	$M1 + (5\pm 3)\% E2$
			0.046 (15)	L_3/L_{12}	0.010	0.989	
			0.243 (20)	M/L_{12}	0.233	0.513	
91.1	3 (1)	16 (8)	5 (3)	α_L	1.13	4.6	$E2 (+ M1)$
105.2	9 (2)	38 (8)	4.2 (13)	α_K	4.58	0.701	$M1 + (10\pm 5)\% E2$
			0.393 (40)	L_{12}/K	0.163	1.87	
			0.124 (25)	L_3/K	0.0015	1.48	
			0.099 (30)	M/K	0.0379	0.862	
111.4	5 (1)	7 (2)	1.5 (5)	α_K	3.89	0.640	$M1 + (75\pm 7)\% E2$
			1.33 (25)	L_{12}/K	0.162	1.59	
			0.73 (25)	L_3/K	0.0012	1.22	
			0.59 (20)	M/K	0.0379	0.723	
116.2	12 (3)	11 (5)	0.9 (4)	α_K	3.44	0.595	$M1 + E2$
118.9	100 (7)	57 (4)	0.57 (6)	α_K	3.22	0.570	$E2$ [norm. ^b]
			1.41 (14)	L_{12}/K	0.162	1.34	
			1.09 (11)	L_3/K	0.0014	0.994	
			0.73 (7)	M/K	0.0378	0.602	
140.8	17 (3)	33 (6)	1.9 (5)	α_K	2.00	0.400	$M1 + (5\pm 4)\% E2$
			0.167 (35)	L_{12}/K	0.161	0.930	
			0.053 (20)	L_3/K	0.0014	0.619	
			0.072 (30)	M/K	0.0376	0.398	
149.7	38 (3)	59 (5)	1.55 (18)	α_K	1.68	0.348	$M1 + (10\pm 5)\% E2$
			0.192 (40)	L_{12}/K	0.161	0.828	
			0.084 (30)	L_3/K	0.0014	0.528	
			0.072 (30)	M/K	0.0376	0.349	
168.6	19 (4)	5.0 (10)	0.11 (3)	α_K	0.490	0.258	$E2$
175.1	28 (4)	4 (2)	0.14 (7)	α_K	E1: 0.079	0.238	(E1)
188.4	30 (4)	2.4 (12)	0.08 (4)	α_K	E1: 0.066	0.198	E1
196.6	13 (4)	5 (3)	0.42 (25)	α_K	0.779	0.178	$M1 + (60\pm 25)\% E2$
			0.38 (10)	L_{12}/K	0.161	0.540	
255.6	16 (3)	1.5 (6)	0.09 (4)	α_K	0.377	0.091	$E2 (+ M1)$
260.3	104 (6)	2.6 (10)	0.025 (10)	α_K	E1: 0.030	0.087	E1
268.5	80 (12)	24 (3)	0.30 (6)	α_K	0.330	0.080	$M1(+ E2)$
			0.19 (6)	L_{12}/K	0.160	0.374	
287.6	17 (3)	4.2 (18)	0.25 (11)	α_K	0.274	0.067	$M1 (+ E2)$
289.8	8 (2)	1.0 (5)	0.12 (6)	α_K	0.268	0.066	$E2, M1 + E2$
307.2	197 (10)	2.7 (10)	0.014 (6)	α_K	E1: 0.020	0.057	E1
313.0	456 (70)	84 (14)	0.19 (4)	α_K	0.218	0.0542	$M1 + (20\pm 6)\% E2$
			0.191 (10)	L_{12}/K	0.160	0.322	
			< 0.024	L_3/K	0.0012	0.101	
			0.057 (10)	M/K	0.037	0.105	
316.2	1018 (55)	180 (10)	0.180 (14)	α_K	0.212	0.0528	$M1 + (20\pm 5)\% E2$
			0.188 (10)	L_{12}/K	0.160	0.319	
			< 0.016	L_3/K	0.0012	0.099	
			0.062 (10)	M/K	0.037	0.104	
320.3	15 (4)	5 (2)	0.33 (14)	α_K	0.204	0.051	$M1$
329.0	593 (90)	87 (14)	0.15 (3)	α_K	0.190	0.0479	$M1 + (30\pm 6)\% E2$
			0.202 (10)	L_{12}/K	0.159	0.308	
			0.020 (8)	L_3/K	0.0012	0.061	
			0.057 (10)	M/K	0.037	0.099	
399.4	36 (2)	5 (2)	0.14 (6)	α_K	0.113	0.030	$M1 (+ E2)$
405.5	42 (5)	3.8 (7)	0.090 (20)	α_K	0.109	0.029	$M1 + (30\pm 30)\% E2$
488.6	58 (5)	2.7 (5)	0.047 (10)	α_K	0.067	0.019	$M1 + (40\pm 20)\% E2$
549.0	27 (8)	1.1 (3)	0.041 (17)	α_K	0.049	0.015	$M1 (+ E2)$
629.6	1800 (80)	42 (2)	0.0233 (15)	α_K	0.0345	0.0108	$M1 + (50\pm 5)\% E2$
645.4	371 (20)	2.8 (9)	0.0075 (24)	α_K	0.0323	0.0103	$E2$
657.4	24 (2)	0.9 (4)	0.038 (17)	α_K	0.0309	0.0099	$M1 (+ E2)$

^aValues interpolated from tabulations by Rösler, Fries, Alder, and Pauli [28].^bSee text for discussion of the normalization of γ -ray intensities to electron intensities.

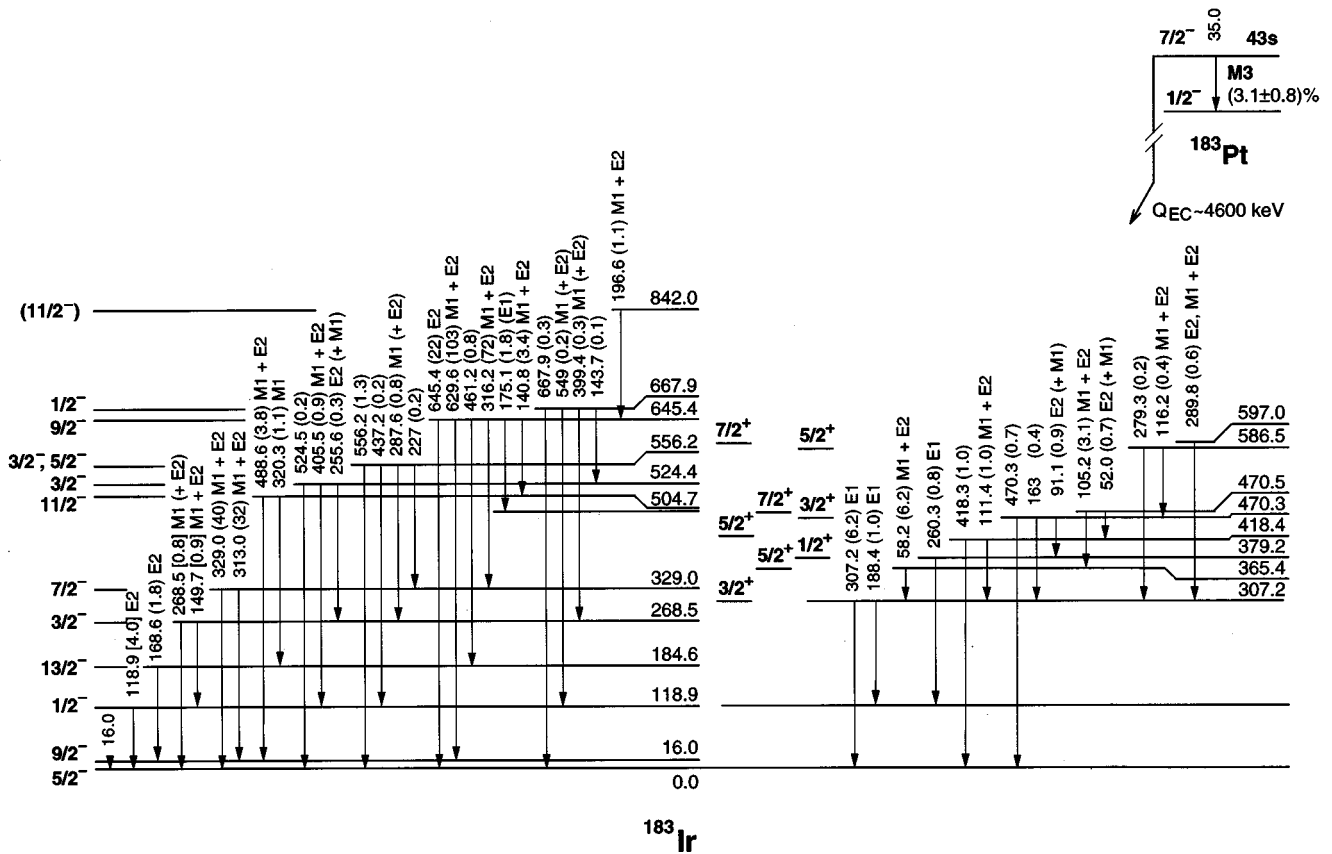


FIG. 10. Low-lying levels in ^{183}Ir populated in the decay of $^{183}\text{Pt}^m$. Level energies and transitions are given in keV. The numbers in parentheses following the transition energies are *total* transition intensities. The transition multiplicities are taken from Table II. The spin-parity assignments are discussed in the text. The details of the $M3$ isomeric transition in ^{183}Pt are taken from Roussière *et al.* [16]. The value for Q_{EC} is taken from the 1993 Atomic Mass Evaluation [26].

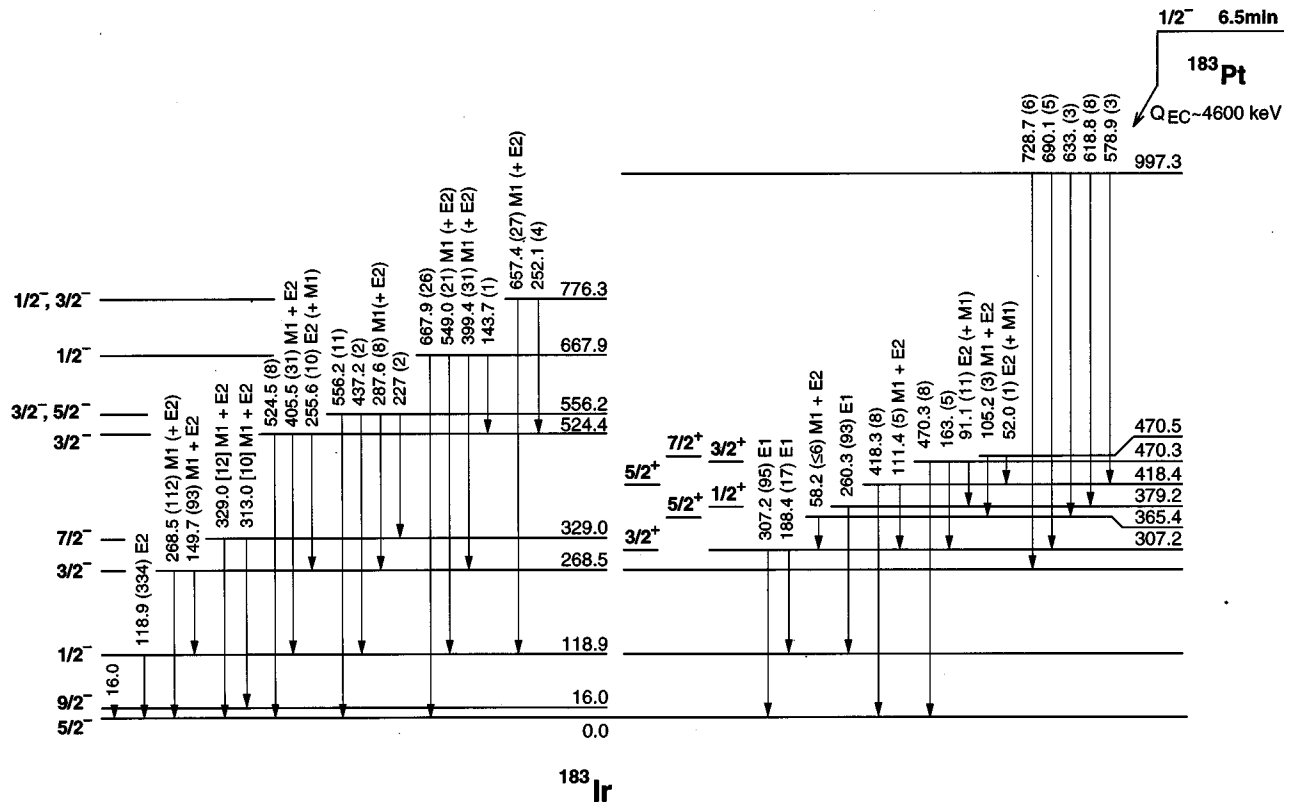


FIG. 11. Low-lying levels in ^{183}Ir populated in the decay of $^{183}\text{Pt}^g$ (cf. caption to Fig. 10).

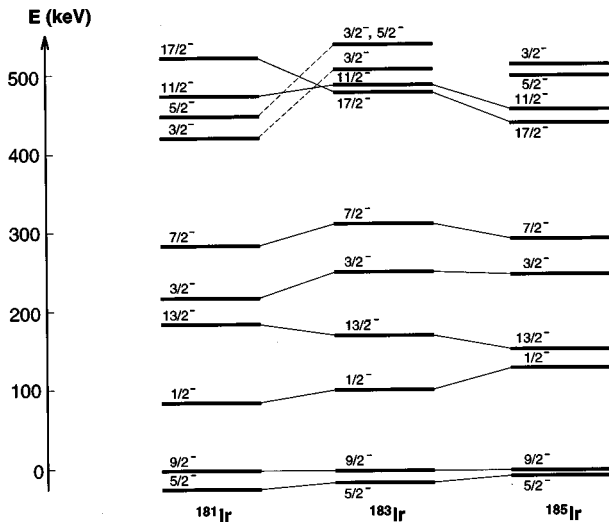


FIG. 12. The systematics of the bands built on the $h_{9/2}$ configuration in $^{181-185}\text{Ir}$, shown relative to the $J^\pi = \frac{9}{2}^-$ state. Data are taken from [3,4,27] and this work.

313.1 keV transition due to the $^{183}\text{Au} \rightarrow ^{183}\text{Pt}$ decay. We avoid this contamination by using coincidence intensities with γ rays and x rays (cf. Figs. 1 and 5). We conclude that the population of the 329.0 keV $\frac{7}{2}^-$ level in the $^{183}\text{Pt}^g$ β decay is probably lower than our implied value.

V. DISCUSSION AND COMPARISON WITH THEORY

The systematics that we deduce for the odd-mass Ir isotopes are shown in Figs. 12–14.

The most notable feature of our study compared with previous studies of ^{183}Ir is the shifting of a whole band of states due to the identification of the strong 58 keV transition lying below the 105 keV transition seen in beam as discussed in the previous section. Indeed, Kreiner *et al.* [8] suggested that such a transition likely existed because of inconsistencies in the bandhead spin parity and decay assigned by Janzen *et al.* [7] and because of inconsistencies with systematics. The present work completely resolves all of these inconsistencies. (We note that the spins assigned by Janzen *et al.*, which

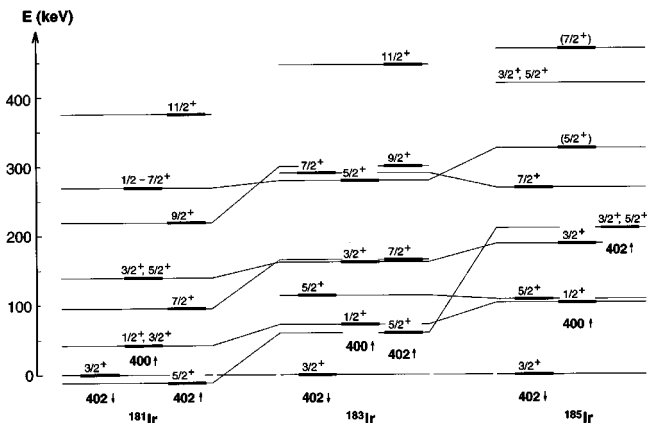


FIG. 13. The systematics of the bands built on the positive parity states in $^{181-185}\text{Ir}$, shown relative to the $\frac{3}{2}^+[402]$ Nilsson configuration. Data are taken from [3,4] and this work.

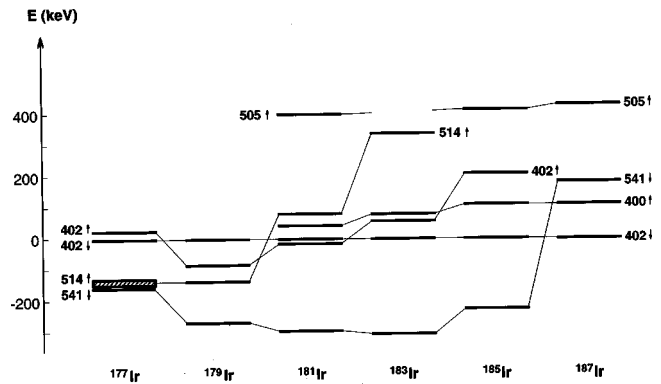


FIG. 14. The systematics of Nilsson (intrinsic) configurations in $^{177-187}\text{Ir}$, shown relative to the $\frac{3}{2}^+[402]$ Nilsson configuration. The $541\downarrow$ configuration is located at the energy of its $J^\pi = \frac{5}{2}^-$ bandhead. Data are taken from [3,4,18–21] and this work.

were supported by deduced $g_K - g_R$ values, remain unchanged: the entire band simply moves on top of the 58 keV transition.) We note also that the earlier systematics for the positive-parity states in the odd-mass Ir isotopes presented by Schück *et al.* [17] and by Sauvage *et al.* [3] must be amended because the lowest positive-parity state in ^{181}Ir has been shown to be $\frac{5}{2}^+[402]$ by Dracoulis *et al.* [4].

A second feature of ^{183}Ir which we consider unresolved is the pattern of excited states that feed the $\frac{9}{2}^-[514]$ state at 645.4 keV. The assignment of this Nilsson configuration, as already noted here and by Visvanathan *et al.* [5], is strongly supported by its very strong β -decay feeding from $^{183}\text{Pt}^m$ which is interpreted as a $\nu \frac{7}{2}^-[514] \rightarrow \pi \frac{9}{2}^-[514]$ transition. However, the band structure reported by Kreiner *et al.* [8] built on the 645.4 keV state does not match the rotational bands built on $\frac{9}{2}^-[514]$ observed in ^{181}Ir [4], ^{179}Ir [21], ^{177}Ir [18], and other odd-Z nuclei in this region [22]. Whereas the $\frac{11}{2}^- \rightarrow \frac{9}{2}^-$ transition energy in $^{177,179,181}\text{Ir}$ is 117 ~ 124 keV, the lowest-energy transition observed by Kreiner *et al.* as feeding the 645.4 keV level has an energy of 197.0 keV. We observe a 196.6 keV transition feeding this level which is possibly the same transition. A possible explanation is provided by Fig. 14, which shows Nilsson bandhead systematics for $^{177-187}\text{Ir}$. Evidently, $\frac{11}{2}^-[505]$ is expected to lie very close (~50 keV) in energy to the $\frac{9}{2}^-[514]$ state. Thus, strong mixing can be expected with consequent distortion of band systematics. Despite a careful search for a low-energy transition corresponding to $\frac{11}{2}^-[505] \rightarrow \frac{9}{2}^-[514]$ we have been unable to provide information on this point. We note that if this transition has an energy near 50 keV, its conversion electrons may be obscured by Ir Auger electrons. We also note a pair of γ rays with energies of 382.2 and 281.5 keV that we assign as feeding the 645.4 keV level in a cascade and the two “bands” that Kreiner *et al.* [8] assign as feeding this level; i.e., there is strong circumstantial evidence for complex band structure built on the 645.4 keV state.

The neutron-deficient odd-mass Ir isotopes have been the subject of a number of detailed theoretical investigations. Besides broadly based investigations using a self-consistent approach [23] and a shell-correction approach [24], detailed particle-rotor model calculations have been made for ^{181}Ir [25] and ^{179}Ir [21]. Taken together, these calculations pro-

